



A model-independent Dalitz plot analysis of $B^\pm \rightarrow DK^\pm$ with $D \rightarrow K_S^0 h^+ h^-$ ($h = \pi, K$) decays and constraints on the CKM angle γ [☆]

LHCb Collaboration

ARTICLE INFO

Article history:

Received 27 September 2012
 Accepted 5 October 2012
 Available online 9 October 2012
 Editor: L. Rolandi

ABSTRACT

A binned Dalitz plot analysis of $B^\pm \rightarrow DK^\pm$ decays, with $D \rightarrow K_S^0 \pi^+ \pi^-$ and $D \rightarrow K_S^0 K^+ K^-$, is performed to measure the CP -violating observables x_\pm and y_\pm which are sensitive to the CKM angle γ . The analysis exploits 1.0 fb^{-1} of data collected by the LHCb experiment. The study makes no model-based assumption on the variation of the strong phase of the D decay amplitude over the Dalitz plot, but uses measurements of this quantity from CLEO-c as input. The values of the parameters are found to be $x_- = (0.0 \pm 4.3 \pm 1.5 \pm 0.6) \times 10^{-2}$, $y_- = (2.7 \pm 5.2 \pm 0.8 \pm 2.3) \times 10^{-2}$, $x_+ = (-10.3 \pm 4.5 \pm 1.8 \pm 1.4) \times 10^{-2}$ and $y_+ = (-0.9 \pm 3.7 \pm 0.8 \pm 3.0) \times 10^{-2}$. The first, second, and third uncertainties are the statistical, the experimental systematic, and the error associated with the precision of the strong-phase parameters measured at CLEO-c, respectively. These results correspond to $\gamma = (44_{-38}^{+43})^\circ$, with a second solution at $\gamma \rightarrow \gamma + 180^\circ$, and $r_B = 0.07 \pm 0.04$, where r_B is the ratio between the suppressed and favoured B decay amplitudes.

© 2012 CERN. Published by Elsevier B.V. Open access under CC BY-NC-ND license.

1. Introduction

A precise determination of the Unitarity Triangle angle γ (also denoted as ϕ_3), is an important goal in flavour physics. Measurements of this weak phase in tree-level processes involving the interference between $b \rightarrow c\bar{u}s$ and $b \rightarrow u\bar{c}s$ transitions are expected to be insensitive to new physics contributions, thereby providing a Standard Model benchmark against which other observables, more likely to be affected by new physics, can be compared. A powerful approach for measuring γ is to study CP -violating observables in $B^\pm \rightarrow DK^\pm$ decays, where D designates a neutral D meson reconstructed in a final state common to both D^0 and \bar{D}^0 decays. Examples of such final states include two-body modes, where LHCb has already presented results [1], and self CP -conjugate three-body decays, such as $K_S^0 \pi^+ \pi^-$ and $K_S^0 K^+ K^-$, designated collectively as $K_S^0 h^+ h^-$.

The proposal to measure γ with $B^\pm \rightarrow DK^\pm$, $D \rightarrow K_S^0 h^+ h^-$ decays was first made in Refs. [2,3]. The strategy relies on comparing the distribution of events in the $D \rightarrow K_S^0 h^+ h^-$ Dalitz plot for $B^+ \rightarrow DK^+$ and $B^- \rightarrow DK^-$ decays. However, in order to determine γ it is necessary to know how the strong phase of the D decay varies over the Dalitz plot. One approach for solving this problem, adopted by BaBar [4–6] and Belle [7–9], is to use an amplitude model fitted on flavour-tagged $D \rightarrow K_S^0 h^+ h^-$ decays to provide this input. An attractive alternative [2,10,11] is to make use of direct measurements of the strong-phase behaviour in bins of the

Dalitz plot, which can be obtained from quantum-correlated $D\bar{D}$ pairs from $\psi(3770)$ decays and that are available from CLEO-c [12], thereby avoiding the need to assign any model-related systematic uncertainty. A first model-independent analysis was recently presented by Belle [13] using $B^\pm \rightarrow DK^\pm$, $D \rightarrow K_S^0 \pi^+ \pi^-$ decays. In this Letter, pp collision data at $\sqrt{s} = 7 \text{ TeV}$, corresponding to an integrated luminosity of 1.0 fb^{-1} and accumulated by LHCb in 2011, are exploited to perform a similar model-independent study of the decay mode $B^\pm \rightarrow DK^\pm$ with $D \rightarrow K_S^0 \pi^+ \pi^-$ and $D \rightarrow K_S^0 K^+ K^-$. The results are used to set constraints on the value of γ .

2. Formalism and external inputs

The amplitude of the decay $B^+ \rightarrow DK^+$, $D \rightarrow K_S^0 h^+ h^-$ can be written as the superposition of the $B^+ \rightarrow \bar{D}^0 K^+$ and $B^+ \rightarrow D^0 K^+$ contributions as

$$A_B(m_+^2, m_-^2) = \bar{A} + r_B e^{i(\delta_B + \gamma)} A. \quad (1)$$

Here m_+^2 and m_-^2 are the invariant masses squared of the $K_S^0 h^+$ and $K_S^0 h^-$ combinations, respectively, that define the position of the decay in the Dalitz plot, $A = A(m_+^2, m_-^2)$ is the $D^0 \rightarrow K_S^0 h^+ h^-$ amplitude, and $\bar{A} = \bar{A}(m_+^2, m_-^2)$ the $\bar{D}^0 \rightarrow K_S^0 h^+ h^-$ amplitude. The parameter r_B , the ratio of the magnitudes of the $B^+ \rightarrow D^0 K^+$ and $B^+ \rightarrow \bar{D}^0 K^+$ amplitudes, is ~ 0.1 [14], and δ_B is the strong-phase difference between them. The equivalent expression for the charge-conjugated decay $B^- \rightarrow DK^-$ is obtained by making the substitutions $\gamma \rightarrow -\gamma$ and $A \leftrightarrow \bar{A}$. Neglecting CP violation, which is known to be small in $D^0 - \bar{D}^0$ mixing and Cabibbo-favoured

[☆] © CERN for the benefit of the LHCb Collaboration.

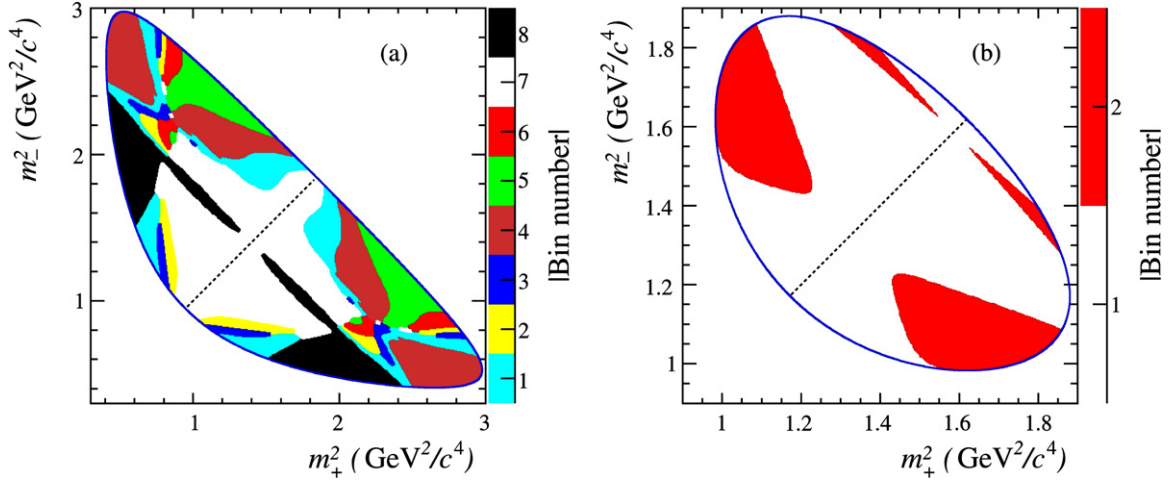


Fig. 1. Binning choices for (a) $D \rightarrow K_S^0 \pi^+ \pi^-$ and (b) $D \rightarrow K_S^0 K^+ K^-$. The diagonal line separates the positive and negative bins.

D meson decays [15], the conjugate amplitudes are related by $A(m_+^2, m_-^2) = \bar{A}(m_-^2, m_+^2)$.

Following the formalism set out in Ref. [2], the Dalitz plot is partitioned into $2N$ regions symmetric under the exchange $m_+^2 \leftrightarrow m_-^2$. The bins are labelled from $-N$ to $+N$ (excluding zero), where the positive bins satisfy $m_-^2 > m_+^2$. At each point in the Dalitz plot, there is a strong-phase difference $\delta_D(m_+^2, m_-^2) = \arg \bar{A} - \arg A$ between the \bar{D}^0 and D^0 decay. The cosine of the strong-phase difference averaged in each bin and weighted by the absolute decay rate is termed c_i and is given by

$$c_i = \frac{\int_{\mathcal{D}_i} (|A| |\bar{A}| \cos \delta_D) d\mathcal{D}}{\sqrt{\int_{\mathcal{D}_i} |A|^2 d\mathcal{D}} \sqrt{\int_{\mathcal{D}_i} |\bar{A}|^2 d\mathcal{D}}}, \quad (2)$$

where the integrals are evaluated over the area \mathcal{D} of bin i . An analogous expression may be written for s_i , which is the sine of the strong-phase difference within bin i , weighted by the decay rate. The values of c_i and s_i can be determined by assuming a functional form for $|A|$, $|\bar{A}|$ and δ_D , which may be obtained from an amplitude model fitted to flavour-tagged D^0 decays. Alternatively direct measurements of c_i and s_i can be used. Such measurements have been performed at CLEO-c, exploiting quantum-correlated $D\bar{D}$ pairs produced at the $\psi(3770)$ resonance. This has been done with a double-tagged method in which one D meson is reconstructed in a decay to either $K_S^0 h^+ h^-$ or $K_1^0 h^+ h^-$, and the other D meson is reconstructed either in a CP eigenstate or in a decay to $K_S^0 h^+ h^-$. The efficiency-corrected event yields, combined with flavour-tag information, allow c_i and s_i to be determined [2, 10, 11]. The latter approach is attractive as it avoids any assumption about the nature of the intermediate resonances which contribute to the $K_S^0 h^+ h^-$ final state; such an assumption leads to a systematic uncertainty associated with the variation in δ_D that is difficult to quantify. Instead, an uncertainty is assigned that is related to the precision of the c_i and s_i measurements.

The population of each positive (negative) bin in the Dalitz plot arising from B^+ decays is N_{+i}^+ (N_{-i}^+), and that from B^- decays is N_{+i}^- (N_{-i}^-). From Eq. (1) it follows that

$$\begin{aligned} N_{\pm i}^+ &= h_{B^+} [K_{\mp i} + (x_+^2 + y_+^2) K_{\pm i} + 2\sqrt{K_i K_{-i}} (x_+ c_{\pm i} \mp y_+ s_{\pm i})], \\ N_{\pm i}^- &= h_{B^-} [K_{\pm i} + (x_-^2 + y_-^2) K_{\mp i} + 2\sqrt{K_i K_{-i}} (x_- c_{\pm i} \pm y_- s_{\pm i})], \end{aligned} \quad (3)$$

where h_{B^\pm} are normalisation factors which can, in principle, be different for B^+ and B^- due to the production asymmetries, and

K_i is the number of events in bin i of the decay of a flavour-tagged $D^0 \rightarrow K_S^0 h^+ h^-$ Dalitz plot. The sensitivity to γ enters through the Cartesian parameters

$$x_{\pm} = r_B \cos(\delta_B \pm \gamma) \quad \text{and} \quad y_{\pm} = r_B \sin(\delta_B \pm \gamma). \quad (4)$$

In this analysis the observed distribution of candidates over the $D \rightarrow K_S^0 h^+ h^-$ Dalitz plot is used to fit x_{\pm} , y_{\pm} and h_{B^\pm} . The parameters c_i and s_i are taken from measurements performed by CLEO-c [12]. In this manner the analysis avoids any dependence on an amplitude model to describe the variation of the strong phase over the Dalitz plot. A model is used, however, to provide the input values for K_i . For the $D^0 \rightarrow K_S^0 \pi^+ \pi^-$ decay the model is taken from Ref. [5] and for the $D^0 \rightarrow K_S^0 K^+ K^-$ decay the model is taken from Ref. [6]. This choice incurs no significant systematic uncertainty as the models have been shown to describe well the intensity distribution of flavour-tagged D^0 decay data.

The effect of $D^0 - \bar{D}^0$ mixing is ignored in the above discussion, and was neglected in the CLEO-c measurements of c_i and s_i as well as in the construction of the amplitude model used to calculate K_i . This leads to a bias of the order of 0.2° in the γ determination [16] which is negligible for the current analysis.

The CLEO-c study segments the $K_S^0 \pi^+ \pi^-$ Dalitz plot into 2×8 bins. Several bin definitions are available. Here the ‘optimal binning’ variant is adopted. In this scheme the bins have been chosen to optimise the statistical sensitivity to γ in the presence of a low level of background, which is appropriate for this analysis. The optimisation has been performed assuming a strong-phase difference distribution as predicted by the BaBar model presented in Ref. [5]. The use of a specific model in defining the bin boundaries does not bias the c_i and s_i measurements. If the model is a poor description of the underlying decay the only consequence will be to reduce the statistical sensitivity of the γ measurement.

For the $K_S^0 K^+ K^-$ final state c_i and s_i measurements are available for the Dalitz plot partitioned into 2×2 , 2×3 and 2×4 bins, with the guiding model being that from the BaBar study described in Ref. [6]. The bin boundaries divide the Dalitz plot into bins of equal size with respect to the strong-phase difference between the D^0 and \bar{D}^0 amplitudes. The current analysis adopts the 2×2 option, a decision driven by the size of the signal sample. The binning choices for the two decay modes are shown in Fig. 1.

3. The LHCb detector

The LHCb detector [17] is a single-arm forward spectrometer covering the pseudorapidity range $2 < \eta < 5$. The detector includes

a high precision tracking system consisting of a silicon-strip vertex detector surrounding the pp interaction region, a large-area silicon-strip detector (VELO) located upstream of a dipole magnet with a bending power of about 4 Tm, and three stations of silicon-strip detectors and straw drift-tubes placed downstream. The combined tracking system has a momentum resolution of (0.4–0.6)% in the range of 5–100 GeV/c, and an impact parameter (IP) resolution of 20 μm for tracks with high transverse momentum (p_T). The dipole magnet can be operated in either polarity and this feature is used to reduce systematic effects due to detector asymmetries. In the data set considered in this analysis, 58% of data were taken with one polarity and 42% with the other. Charged hadrons are identified using two ring-imaging Cherenkov (RICH) detectors. Photon, electron and hadron candidates are identified by a calorimeter system consisting of scintillating-pad and preshower detectors, an electromagnetic calorimeter and a hadronic calorimeter. Muons are identified by a system composed of alternating layers of iron and multiwire proportional chambers.

A two-stage trigger is employed. First a hardware-based decision is taken at a frequency up to 40 MHz. It accepts high transverse energy clusters in either the electromagnetic calorimeter or hadron calorimeter, or a muon of high p_T . For this analysis, it is required that one of the charged final-state tracks forming the B^\pm candidate points at a deposit in the hadron calorimeter, or that the hardware-trigger decision was taken independently of these tracks. A second trigger level, implemented in software, receives 1 MHz of events and retains $\sim 0.3\%$ of them [18]. It searches for a track with large p_T and large IP with respect to any pp interaction point which is called a primary vertex (PV). This track is then required to be part of a two-, three- or four-track secondary vertex with a high p_T sum, significantly displaced from any PV. In order to maximise efficiency at an acceptable trigger rate, the displaced vertex is selected with a decision tree algorithm that uses p_T , impact parameter, flight distance and track separation information. Full event reconstruction occurs offline, and a loose preselection is applied.

Approximately three million simulated events for each of the modes $B^\pm \rightarrow D(K_S^0 \pi^+ \pi^-) K^\pm$ and $B^\pm \rightarrow D(K_S^0 \pi^+ \pi^-) \pi^\pm$, and one million simulated events for each of $B^\pm \rightarrow D(K_S^0 K^+ K^-) K^\pm$ and $B^\pm \rightarrow D(K_S^0 K^+ K^-) \pi^\pm$ are used in the analysis, as well as a large inclusive sample of generic $B \rightarrow DX$ decays for background studies. These samples are generated using a version of PYTHIA 6.4 [19] tuned to model the pp collisions [20]. EVTGEN [21] encodes the particle decays in which final state radiation is generated using PHOTOS [22]. The interaction of the generated particles with the detector and its response are implemented using the GEANT4 toolkit [23] as described in Ref. [24].

4. Event selection and invariant mass spectrum fit

Selection requirements are applied to isolate both $B^\pm \rightarrow DK^\pm$ and $B^\pm \rightarrow D\pi^\pm$ candidates, with $D \rightarrow K_S^0 h^+ h^-$. Candidates selected in the Cabibbo-favoured $B^\pm \rightarrow D\pi^\pm$ decay mode provide an important control sample which is exploited in the analysis.

A production vertex is assigned to each B candidate. This is the PV for which the reconstructed B trajectory has the smallest IP χ^2 , where this quantity is defined as the difference in the χ^2 fit of the PV with and without the tracks of the considered particle. The K_S^0 candidates are formed from two oppositely charged tracks reconstructed in the tracking stations, either with associated hits in the VELO detector (long K_S^0 candidate) or without (downstream K_S^0 candidate). The IP χ^2 with respect to the PV of each of the long (downstream) K_S^0 daughters is required to be greater than 16 (4). The angle θ between the K_S^0 candidate momentum and the vector between the decay vertex and the PV, expected to be small

given the high momentum of the B meson, is required to satisfy $\cos\theta > 0.99$, reducing background from combinations of random tracks.

The D meson candidates are reconstructed by combining the long (downstream) K_S^0 candidates with two oppositely charged tracks for which the values of the IP χ^2 with respect to the PV are greater than 9 (16). In the case of the $D \rightarrow K_S^0 K^+ K^-$ a loose particle identification (PID) requirement is placed on the kaons to reduce combinatoric backgrounds. The IP χ^2 of the candidate D with respect to any PV is demanded to be greater than 9 in order to suppress directly produced D mesons, and the angle θ between the D candidate momentum and the vector between the decay and PV is required to satisfy the same criterion as for the K_S^0 selection ($\cos\theta > 0.99$). The invariant mass resolution of the signal is 8.7 MeV/ c^2 (11.9 MeV/ c^2) for D mesons reconstructed with long (downstream) K_S^0 candidates, and a common window of ± 25 MeV/ c^2 is imposed around the world average D^0 mass [15]. The K_S^0 mass is determined after the addition of a constraint that the invariant mass of the two D daughter pions or kaons and the two K_S^0 daughter pions have the world average D mass. The invariant mass resolution is 2.9 MeV/ c^2 (4.8 MeV/ c^2) for long (downstream) K_S^0 decays. Candidates are retained for which the invariant mass of the two K_S^0 daughters lies within ± 15 MeV/ c^2 of the world average K_S^0 mass [15].

The D meson is combined with a candidate kaon or pion bachelor particle to form the B candidate. The IP χ^2 of the bachelor with respect to the PV is required to be greater than 25. In order to ensure good discrimination between pions and kaons in the RICH system only tracks with momentum less than 100 GeV/c are considered. The bachelor is considered as a candidate kaon (pion) according to whether it passes (fails) a cut placed on the output of the RICH PID algorithm. The PID information is quantified as a difference between the logarithm of the likelihood under the mass hypothesis of a pion or a kaon. Criteria are then imposed on the B candidate: that the angle between its momentum and the vector between the decay and the PV should have a cosine greater than 0.9999 for candidates containing long K_S^0 decays (0.99995 for downstream K_S^0 decays); that the B vertex-separation χ^2 with respect to its PV is greater than 169; and that the B IP χ^2 with respect to the PV is less than 9. To suppress background from charmless B decays it is required that the D vertex lies downstream of the B vertex. In the events with a long K_S^0 candidate, a further background arises from $B^\pm \rightarrow Dh^\pm$, $D \rightarrow \pi^+ \pi^- h^+ h^-$ decays, where the two pions are reconstructed as a long K_S^0 candidate. This background is removed by requiring that the flight significance between the D and K_S^0 vertices is greater than 10.

In order to obtain the best possible resolution in the Dalitz plot of the D decay, and to provide further background suppression, the B , D and K_S^0 vertices are refitted with additional constraints on the D and K_S^0 masses, and the B momentum is required to point back to the PV. The χ^2 per degree of freedom of the fit is required to be less than 5.

Less than 0.4% of the selected events are found to contain two or more candidates. In these events only the B candidate with the lowest χ^2 per degree of freedom from the refit is retained for subsequent study. In addition, 0.4% of the candidates are found to have been reconstructed such that their D Dalitz plot coordinates lie outside the defined bins, and these too are discarded.

The invariant mass distributions of the selected candidates are shown in Fig. 2 for $B^\pm \rightarrow DK^\pm$ and $B^\pm \rightarrow D\pi^\pm$, with $D \rightarrow K_S^0 \pi^+ \pi^-$ decays, divided between the long and downstream K_S^0 categories. Fig. 3 shows the corresponding distributions for final states with $D \rightarrow K_S^0 K^+ K^-$, here integrated over the two K_S^0 categories. The result of an extended, unbinned, maximum likelihood

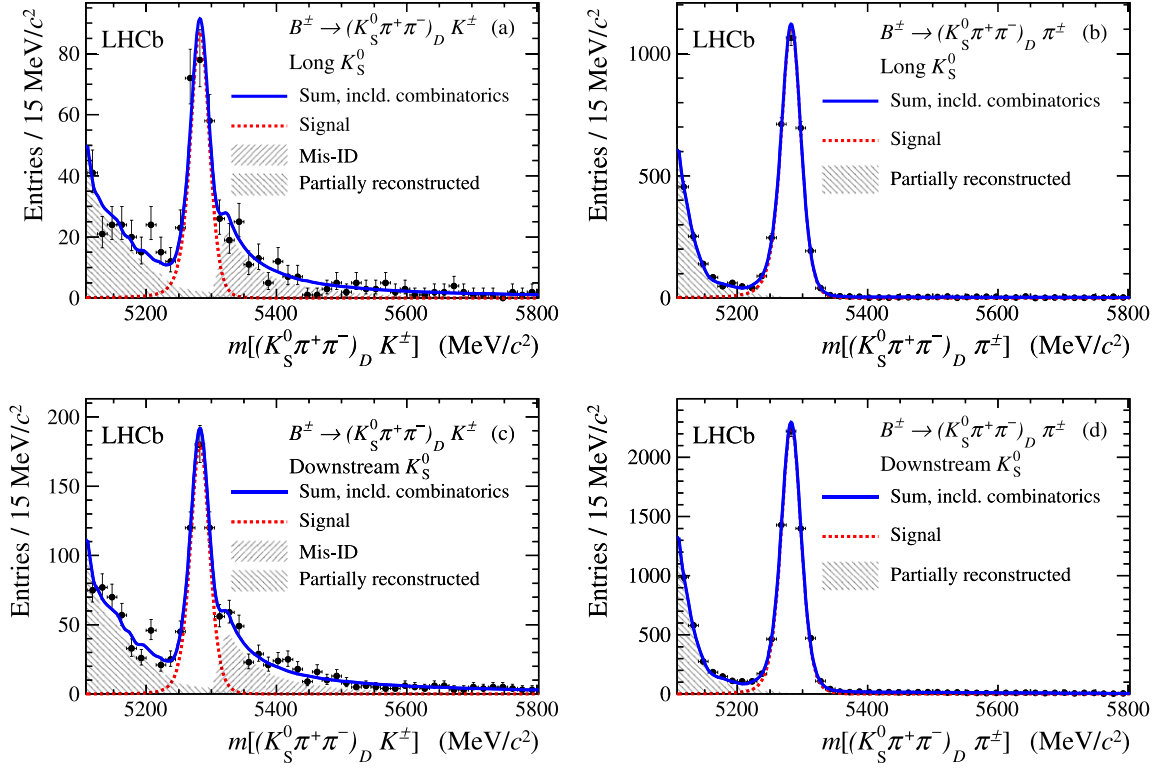


Fig. 2. Invariant mass distributions of (a, c) $B^\pm \rightarrow DK^\pm$ and (b, d) $B^\pm \rightarrow D\pi^\pm$ candidates, with $D \rightarrow K_S^0 \pi^+ \pi^-$, divided between the (a, b) long and (c, d) downstream K_S^0 categories. Fit results, including the signal and background components, are superimposed.

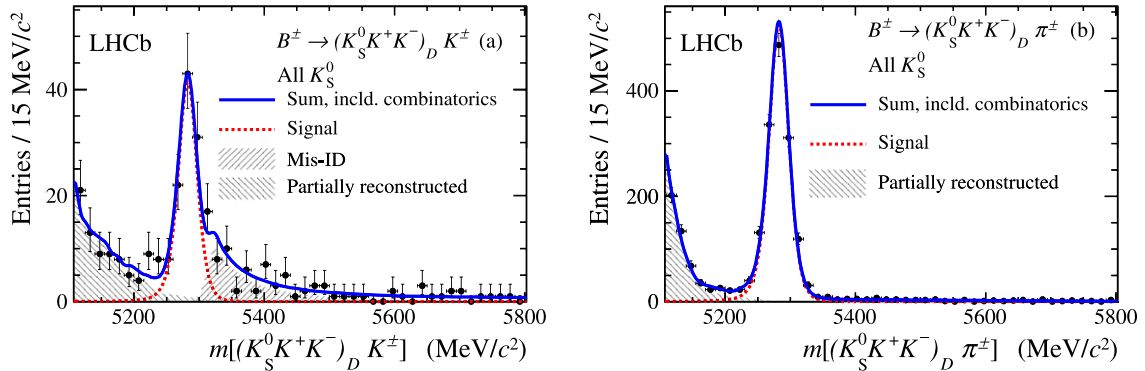


Fig. 3. Invariant mass distributions of (a) $B^\pm \rightarrow DK^\pm$ and (b) $B^\pm \rightarrow D\pi^\pm$ candidates, with $D \rightarrow K_S^0 K^+ K^-$, shown with both K_S^0 categories combined. Fit results, including the signal and background components, are superimposed.

fit to these distributions is superimposed. The fit is performed simultaneously for $B^\pm \rightarrow DK^\pm$ and $B^\pm \rightarrow D\pi^\pm$, including both $D \rightarrow K_S^0 \pi^+ \pi^-$ and $D \rightarrow K_S^0 K^+ K^-$ decays, allowing several parameters to be different for long and downstream K_S^0 categories. The fit range is between 5110 MeV/c^2 and 5800 MeV/c^2 in invariant mass. At this stage in the analysis the fit does not distinguish between the different regions of Dalitz plot or B meson charge. The purpose of this global fit is to determine the parameters that describe the invariant mass spectrum in preparation for the binned fit described in Section 5.

The signal probability density function (PDF) is a Gaussian function with asymmetric tails where the unnormalised form is given by

$$f(m; m_0, \alpha_L, \alpha_R, \sigma) = \begin{cases} \exp[-(m - m_0)^2 / (2\sigma^2 + \alpha_L(m - m_0)^2)], & m < m_0; \\ \exp[-(m - m_0)^2 / (2\sigma^2 + \alpha_R(m - m_0)^2)], & m > m_0; \end{cases} \quad (5)$$

where m is the candidate mass, m_0 the B mass and σ , α_L , and α_R are free parameters in the fit. The parameter m_0 is taken as common for all classes of signal. The parameters describing the asymmetric tails are fitted separately for events with long and downstream K_S^0 categories. The resolution of the Gaussian function is left as a free parameter for the two K_S^0 categories, but the ratio between this resolution in $B^\pm \rightarrow DK^\pm$ and $B^\pm \rightarrow D\pi^\pm$ decays is required to be the same, independent of category. The resolution is determined to be around 15 MeV/c^2 for $B^\pm \rightarrow D\pi^\pm$ decays of both K_S^0 classes, and is smaller by a factor 0.95 ± 0.06 for $B^\pm \rightarrow DK^\pm$. The yield of $B^\pm \rightarrow D\pi^\pm$ candidates in each category is determined in the fit. Instead of fitting the yield of the $B^\pm \rightarrow DK^\pm$ candidates separately, the ratio $\mathcal{R} = N(B^\pm \rightarrow DK^\pm) / N(B^\pm \rightarrow D\pi^\pm)$ is a free parameter and is common across all categories.

The background has contributions from random track combinations and partially reconstructed B decays. The random track combinations are modelled by linear PDFs, the parameters of which are

Table 1

Yields and statistical uncertainties in the signal region from the invariant mass fit, scaled from the full fit mass range, for candidates passing the $B^\pm \rightarrow Dh^\pm$, $D \rightarrow K_S^0 \pi^+ \pi^-$ selection. Values are shown separately for candidates containing long and downstream K_S^0 decays. The signal region is between 5247 MeV/ c^2 and 5317 MeV/ c^2 and the full fit range is between 5110 MeV/ c^2 and 5800 MeV/ c^2 .

Fit component	$B^\pm \rightarrow DK^\pm$ selection		$B^\pm \rightarrow D\pi^\pm$ selection	
	Long	Downstream	Long	Downstream
$B^\pm \rightarrow DK^\pm$	213 ± 13	441 ± 25	–	–
$B^\pm \rightarrow D\pi^\pm$	11 ± 3	22 ± 5	2809 ± 56	5755 ± 82
Combinatoric	9 ± 4	29 ± 6	22 ± 3	90 ± 7
Partially reconstructed	11 ± 1	25 ± 2	25 ± 1	55 ± 1

Table 2

Yields and statistical uncertainties in the signal region from the invariant mass fit, scaled from the full fit mass range, for candidates passing the $B^\pm \rightarrow Dh^\pm$, $D \rightarrow K_S^0 K^+ K^-$ selection. Values are shown separately for candidates containing long and downstream K_S^0 decays. The signal region is between 5247 MeV/ c^2 and 5317 MeV/ c^2 and the full fit range is between 5110 MeV/ c^2 and 5800 MeV/ c^2 .

Fit component	$B^\pm \rightarrow DK^\pm$ selection		$B^\pm \rightarrow D\pi^\pm$ selection	
	Long	Downstream	Long	Downstream
$B^\pm \rightarrow DK^\pm$	32 ± 2	70 ± 4	–	–
$B^\pm \rightarrow D\pi^\pm$	1.6 ± 1.2	3.4 ± 1.8	417 ± 20	913 ± 29
Combinatoric	0.6 ± 0.5	2.5 ± 0.9	4.8 ± 1.4	18 ± 2
Partially reconstructed	2.2 ± 0.4	2.9 ± 0.5	3.7 ± 0.3	7.7 ± 0.5

floated separately for each class of decay. Partially reconstructed backgrounds are described empirically. Studies of simulated events show that the partially reconstructed backgrounds are dominated by decays that involve a D meson decaying to $K_S^0 h^+ h^-$. Therefore the same PDF is used to describe these backgrounds as used in a similar analysis of $B^\pm \rightarrow DK^\pm$ decays, with $D \rightarrow K^\pm \pi^\mp$, $K^+ K^-$ and $\pi^+ \pi^-$ [1]. In that analysis the shape was constructed by applying the selection to a large simulated sample containing many common backgrounds, each weighted by its production rate and branching fraction. The invariant mass distribution for the surviving candidates was corrected to account for small differences in resolution and PID performance between data and simulation, and two background PDFs were extracted by kernel estimation [25]; one for $B^\pm \rightarrow DK^\pm$ and one for $B^\pm \rightarrow D\pi^\pm$ decays. The partially reconstructed background PDFs are found to give a good description of both K_S^0 categories.

An additional and significant background component exists in the $B^\pm \rightarrow DK^\pm$ sample, arising from the dominant $B^\pm \rightarrow D\pi^\pm$ decay on those occasions where the bachelor particle is misidentified as a kaon by the RICH system. In contrast, the $B^\pm \rightarrow DK^\pm$ contamination in the $B^\pm \rightarrow D\pi^\pm$ sample can be neglected. The size of this background is calculated through knowledge of PID and misidentification efficiencies, which are obtained from large samples of kinematically selected $D^{*\pm} \rightarrow D\pi^\pm$, $D \rightarrow K^\mp \pi^\pm$ decays. The kinematic properties of the particles in the calibration sample are reweighted to match those of the bachelor particles in the B decay sample, thereby ensuring that the measured PID performance is representative of that in the B decay sample. The efficiency to identify a kaon correctly is found to be around 86%, and that for a pion to be around 96%. The misidentification efficiencies are the complements of these numbers. From this information and from knowledge of the number of reconstructed $B^\pm \rightarrow D\pi^\pm$ decays, the amount of this background surviving the $B^\pm \rightarrow DK^\pm$ selection can be determined. The invariant mass distribution of the misidentified candidates is described by a Crystal Ball function [26] with the tail on the high mass side, the parameters of which are fitted in common between all the $B^\pm \rightarrow DK^\pm$ samples.

The number of $B^\pm \rightarrow DK^\pm$ candidates in all categories is determined by \mathcal{R} , and the number of $B^\pm \rightarrow D\pi^\pm$ events in the corresponding category. The ratio \mathcal{R} is determined in the fit and measured to be 0.085 ± 0.005 (statistical uncertainty only) and is consistent with that observed in Ref. [1]. The yields returned by

the invariant mass fit in the full fit region are scaled to the signal region, defined as 5247–5317 MeV/ c^2 , and are presented in Tables 1 and 2 for the $D \rightarrow K_S^0 \pi^+ \pi^-$ and $D \rightarrow K_S^0 K^+ K^-$ selections respectively. In the $B^\pm \rightarrow D(K_S^0 \pi^+ \pi^-) K^\pm$ sample there are 654 ± 28 signal candidates, with a purity of 86%. The corresponding numbers for the $B^\pm \rightarrow D(K_S^0 K^+ K^-) K^\pm$ sample are 102 ± 5 and 88%, respectively. The contamination in the $B^\pm \rightarrow DK^\pm$ selection receives approximately equal contributions from misidentified $B^\pm \rightarrow D\pi^\pm$ decays, combinatoric background and partially reconstructed decays. The partially reconstructed component in the signal region is dominated by decays of the type $B \rightarrow D\rho$, in which a charged pion from the ρ decay is misidentified as the bachelor kaon, and $B^\pm \rightarrow D^* \pi^\pm$, again with a misidentified pion.

The Dalitz plots for $B^\pm \rightarrow DK^\pm$ data in the signal region for the two $D \rightarrow K_S^0 h^+ h^-$ final states are shown in Fig. 4. Separate plots are shown for B^+ and B^- decays.

5. Binned Dalitz fit

The purpose of the binned Dalitz plot fit is to measure the CP -violating parameters x_\pm and y_\pm , as introduced in Section 2. Following Eq. (3) these parameters can be determined from the populations of each $B^\pm \rightarrow DK^\pm$ Dalitz plot bin given the external information that is available for the c_i , s_i and K_i parameters. In order to know the signal population in each bin it is necessary both to subtract background and to correct for acceptance losses from the trigger, reconstruction and selection.

Although the absolute numbers of B^+ and B^- decays integrated over the Dalitz plot have some dependence on x_\pm and y_\pm , the additional sensitivity gained compared to using just the relative bin-to-bin yields is negligible, and is therefore not used. Consequently the analysis is insensitive to any B production asymmetries, and only knowledge of the relative acceptance is required. The relative acceptance is determined from the control channel $B^\pm \rightarrow D\pi^\pm$. In this decay the ratio of $b \rightarrow u\bar{c}d$ to $b \rightarrow \bar{c}u\bar{d}$ amplitudes is expected to be very small (~ 0.005) and thus, to a good approximation, interference between the transitions can be neglected. Hence the relative population of decays expected in each $B^\pm \rightarrow D\pi^\pm$ Dalitz plot bin can be predicted using the K_i values calculated with the $D \rightarrow K_S^0 h^+ h^-$ model. Dividing the background-subtracted yield observed in each bin by this prediction enables the relative acceptance to be determined, and then applied to the $B^\pm \rightarrow DK^\pm$ data.

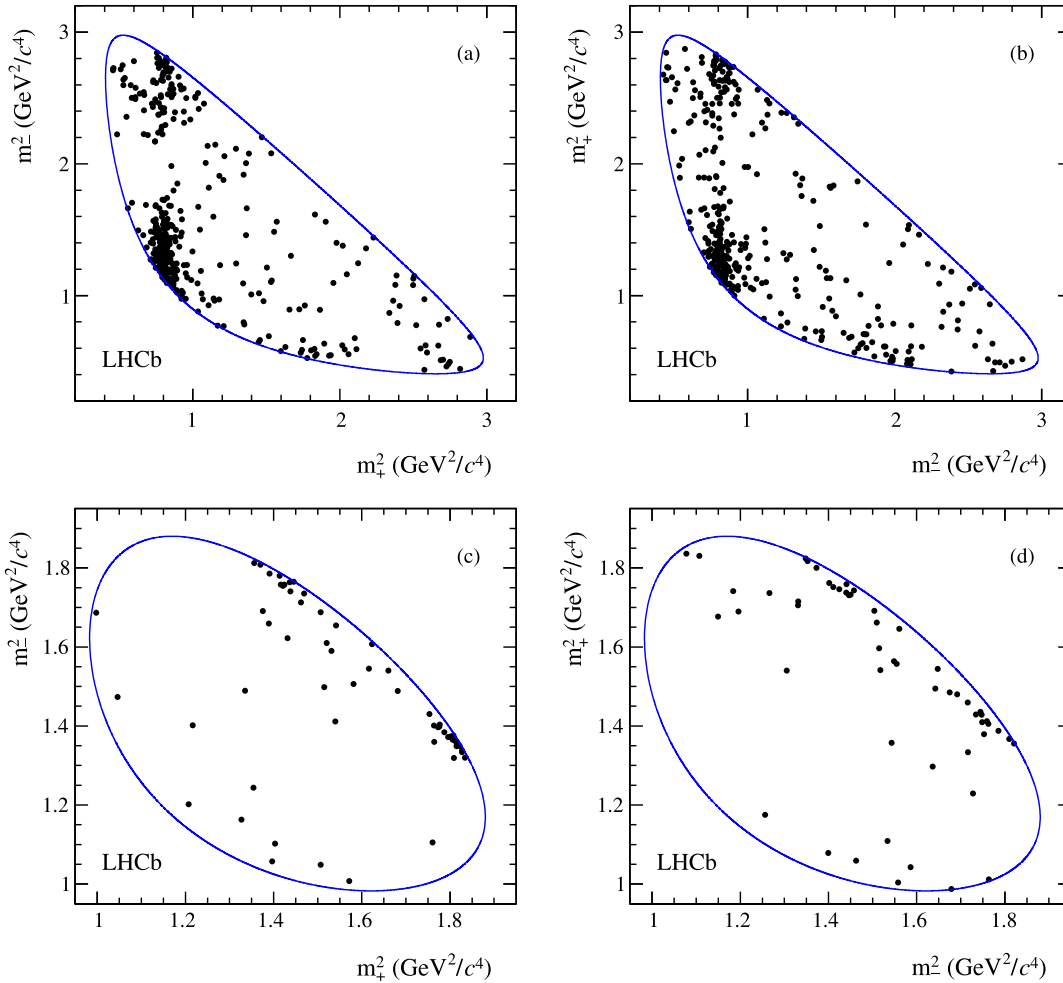


Fig. 4. Dalitz plots of $B^\pm \rightarrow DK^\pm$ candidates in the signal region for (a, b) $D \rightarrow K_S^0 \pi^+ \pi^-$ and (c, d) $D \rightarrow K_S^0 K^+ K^-$ decays, divided between (a, c) B^+ and (b, d) B^- . The boundaries of the kinematically-allowed regions are also shown.

In order to optimise the statistical precision of this procedure, the bins $+i$ and $-i$ are combined in the calculation, since the efficiencies in these symmetric regions are expected to be the same in the limit that there are no charge-dependent reconstruction asymmetries. It is found that the variation in relative acceptance between non-symmetric bins is at most $\sim 50\%$, with the lowest efficiency occurring in those regions where one of the pions has low momentum.

Separate fits are performed to the B^+ and B^- data. Each fit simultaneously considers the two K_S^0 categories, the $B^\pm \rightarrow DK^\pm$ and $B^\pm \rightarrow D\pi^\pm$ candidates, and the two $D \rightarrow K_S^0 h^+ h^-$ final states. In order to assess the impact of the $D \rightarrow K_S^0 K^+ K^-$ data the fit is then repeated including only the $D \rightarrow K_S^0 \pi^+ \pi^-$ sample. The PDF parameters for both the signal and background invariant mass distributions are fixed to the values determined in the global fit. The yields of all the background contributions in each bin are free parameters, apart from bins where a very low contribution is determined from an initial fit, in which case they are fixed to zero, to facilitate the calculation of the error matrix. The yields of signal candidates for each bin in the $B^\pm \rightarrow D\pi^\pm$ sample are also free parameters. The amount of signal in each bin for the $B^\pm \rightarrow DK^\pm$ sample is determined by varying the integrated yield and the x_\pm and y_\pm parameters.

A large ensemble of simulated experiments are performed to validate the fit procedure. In each experiment the number and distribution of signal and background candidates are generated

according to the expected distribution in data, and the full fit procedure is then executed. The values for x_\pm and y_\pm are set close to those determined by previous measurements [14]. It is found from this exercise that the errors are well estimated. Small biases are, however, observed in the central values returned by the fit and these are applied as corrections to the results obtained on data. The bias is $(0.2\text{--}0.3) \times 10^{-2}$ for most parameters but rises to 1.0×10^{-2} for y_+ . This bias is due to the low yields in some of the bins and is an inherent feature of the maximum likelihood fit. This behaviour is associated with the size of data set being fit, since when simulated experiments are performed with larger sample sizes the biases are observed to reduce.

The results of the fits are presented in Table 3. The systematic uncertainties are discussed in Section 6. The statistical uncertainties are compatible with those predicted by simulated experiments. The inclusion of the $D \rightarrow K_S^0 K^+ K^-$ data improves the precision on x_\pm by around 10%, and has little impact on y_\pm . This behaviour is expected, as the measured values of c_i in this mode, which multiply x_\pm in Eq. (4), are significantly larger than those of s_i , which multiply y_\pm . The two sets of results are compatible within the statistical and uncorrelated systematic uncertainties.

The measured values of (x_\pm, y_\pm) from the fit to all data, with their statistical likelihood contours are shown in Fig. 5. The expected signature for a sample that exhibits CP violation is that the two vectors defined by the coordinates (x_-, y_-) and (x_+, y_+) should both be non-zero in magnitude, and have different phases.

Table 3

Results for x_{\pm} and y_{\pm} from the fits to the data in the case when both $D \rightarrow K_S^0 \pi^+ \pi^-$ and $D \rightarrow K_S^0 K^+ K^-$ are considered and when only the $D \rightarrow K_S^0 \pi^+ \pi^-$ final state is included. The first, second, and third uncertainties are the statistical, the experimental systematic, and the error associated with the precision of the strong-phase parameters, respectively. The correlation coefficients are calculated including all sources of uncertainty (the values in parentheses correspond to the case where only the statistical uncertainties are considered).

Parameter	All data	$D \rightarrow K_S^0 \pi^+ \pi^-$ alone
$x_- [\times 10^{-2}]$	$0.0 \pm 4.3 \pm 1.5 \pm 0.6$	$1.6 \pm 4.8 \pm 1.4 \pm 0.8$
$y_- [\times 10^{-2}]$	$2.7 \pm 5.2 \pm 0.8 \pm 2.3$	$1.4 \pm 5.4 \pm 0.8 \pm 2.4$
$\text{corr}(x_-, y_-)$	$-0.10 (-0.11)$	$-0.12 (-0.12)$
$x_+ [\times 10^{-2}]$	$-10.3 \pm 4.5 \pm 1.8 \pm 1.4$	$-8.6 \pm 5.4 \pm 1.7 \pm 1.6$
$y_+ [\times 10^{-2}]$	$-0.9 \pm 3.7 \pm 0.8 \pm 3.0$	$-0.3 \pm 3.7 \pm 0.9 \pm 2.7$
$\text{corr}(x_+, y_+)$	$0.22 (0.17)$	$0.20 (0.17)$

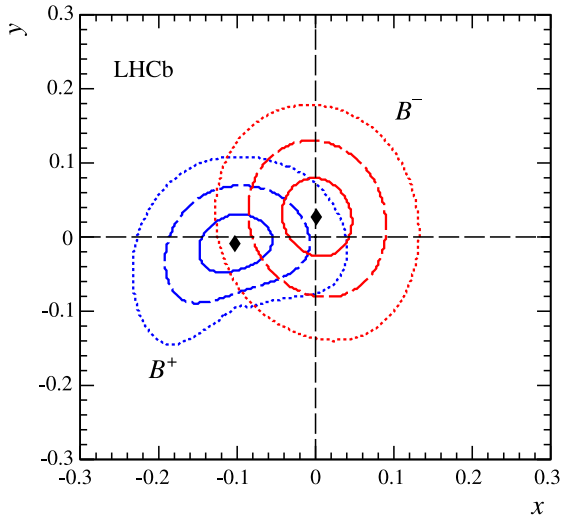


Fig. 5. One (solid), two (dashed) and three (dotted) standard deviation confidence levels for (x_+, y_+) (blue) and (x_-, y_-) (red) as measured in $B^{\pm} \rightarrow DK^{\pm}$ decays (statistical only). The points represent the best fit central values. (For interpretation of the references to colour in this figure legend, the reader is referred to the web version of this Letter.)

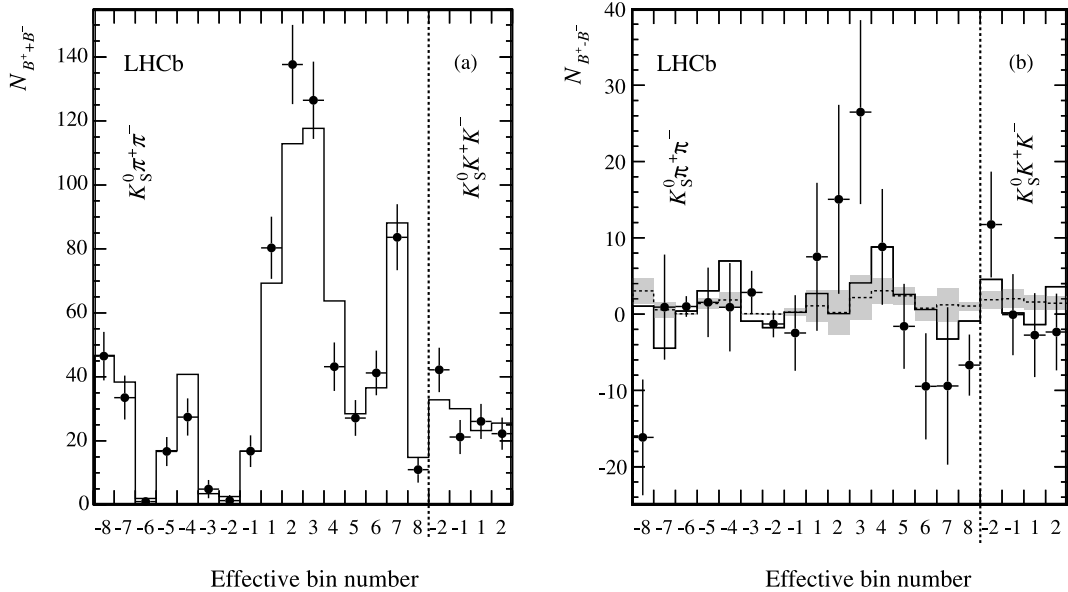


Fig. 6. Signal yield in effective bins compared with prediction of (x_{\pm}, y_{\pm}) fit (black histogram) for $D \rightarrow K_S^0 \pi^+ \pi^-$ and $D \rightarrow K_S^0 K^+ K^-$. Figure (a) shows the sum of B^+ and B^- yields. Figure (b) shows the difference of B^+ and B^- yields. Also shown (dashed line and grey shading) is the expectation and uncertainty for the zero CP violation hypothesis.

The data show this behaviour, but are also compatible with the no CP violation hypothesis.

In order to investigate whether the binned fit gives an adequate description of the data, a study is performed to compare the observed number of signal candidates in each bin with that expected given the fitted total yield and values of x_{\pm} and y_{\pm} . The number of signal candidates is determined by fitting in each bin for the $B^{\pm} \rightarrow DK^{\pm}$ contribution for long and downstream K_S^0 decays combined, with no assumption on how this component is distributed over the Dalitz plot. Fig. 6 shows the results in effective bin number separately for $N_{B^+ + B^-}$, the sum of B^+ and B^- candidates, which is a CP -conserving observable, and for the difference $N_{B^+ - B^-}$, which is sensitive to CP violation. The effective bin number is equal to the normal bin number for B^+ , but is defined to be this number multiplied by -1 for B^- . The expectations from the (x_{\pm}, y_{\pm}) fit are superimposed as is, for the $N_{B^+ + B^-}$ distribution, the prediction for the case $x_{\pm} = y_{\pm} = 0$. Note that the zero CP violation prediction is not a horizontal line at $N_{B^+ - B^-} = 0$ because it is calculated using the total B^+ and B^- yields from the full fit, and using bin efficiencies that are determined separately for each sample. The data and fit expectations are compatible for both distributions yielding a χ^2 probability of 10% for $N_{B^+ + B^-}$ and 34% for $N_{B^+ - B^-}$. The results for the $N_{B^+ - B^-}$ distribution are also compatible with the no CP violation hypothesis (χ^2 probability = 16%).

6. Systematic uncertainties

Systematic uncertainties are evaluated for the fits to the full data sample and are presented in Table 4. In order to understand the impact of the CLEO-c (c_i, s_i) measurements the errors arising from this source are kept separate from the other experimental uncertainties. Table 5 shows the uncertainties for the case where only $D \rightarrow K_S^0 \pi^+ \pi^-$ decays are included. Each contribution to the systematic uncertainties is now discussed in turn.

The uncertainties on the shape parameters of the invariant mass distributions as determined from the global fit when propagated through to the binned analysis induce uncertainties on x_{\pm} and y_{\pm} . In addition, consideration is given to certain assumptions

Table 4

Summary of statistical, experimental and strong-phase uncertainties on x_{\pm} and y_{\pm} in the case where both $D \rightarrow K_S^0 \pi^+ \pi^-$ and $D \rightarrow K_S^0 K^+ K^-$ decays are included in the fit. All entries are given in multiples of 10^{-2} .

Component	$\sigma(x_-)$	$\sigma(y_-)$	$\sigma(x_+)$	$\sigma(y_+)$
Statistical	4.3	5.2	4.5	3.7
Global fit shape parameters	0.4	0.4	0.6	0.4
Efficiency effects	0.3	0.4	0.3	0.4
CP violation in control mode	1.3	0.4	1.5	0.2
Migration	0.4	0.2	0.4	0.2
Partially reconstructed background	0.2	0.3	0.2	0.2
PID efficiency	0.1	0.2	0.2	< 0.1
Shape of misidentified $B^{\pm} \rightarrow D\pi^{\pm}$	0.1	0.1	0.3	< 0.1
Bias correction	0.2	0.3	0.2	0.5
Total experimental systematic	1.5	0.9	1.8	0.8
Strong-phase systematic	0.6	2.3	1.4	3.0

Table 5

Summary of statistical, experimental and strong-phase uncertainties on x_{\pm} and y_{\pm} in the case where only $D \rightarrow K_S^0 \pi^+ \pi^-$ decays are included in the fit. All entries are given in multiples of 10^{-2} .

Component	$\sigma(x_-)$	$\sigma(y_-)$	$\sigma(x_+)$	$\sigma(y_+)$
Statistical	4.8	5.4	5.4	3.7
Global fit shape parameters	0.4	0.4	0.6	0.4
Efficiency effects	0.2	0.2	0.3	0.4
CP violation in control mode	1.2	0.5	1.5	0.2
Migration	0.4	0.2	0.4	0.2
Partially reconstructed background	0.1	0.1	0.3	0.2
PID efficiency	< 0.1	0.2	< 0.1	< 0.1
Shape of misidentified $B^{\pm} \rightarrow D\pi^{\pm}$	0.1	< 0.1	0.1	< 0.1
Bias correction	0.2	0.3	0.2	0.6
Total experimental systematic	1.4	0.8	1.7	0.9
Strong-phase systematic	0.8	2.4	1.6	2.7

made in the fit. For example, the slope of the combinatoric background in the data set containing $D \rightarrow K_S^0 K^+ K^-$ decays is fixed to be zero on account of the limited sample size. The induced errors associated with these assumptions are evaluated and found to be small compared to those coming from the parameter uncertainties themselves, which vary between 0.4×10^{-2} and 0.6×10^{-2} for the fit to the full data sample.

The analysis assumes an efficiency that is flat across each Dalitz plot bin. In reality the efficiency varies, and this leads to a potential bias in the determination of x_{\pm} and y_{\pm} , since the non-uniform acceptance means that the values of (c_i, s_i) appropriate for the analysis can differ from those corresponding to the flat-efficiency case. The possible size of this effect is evaluated in LHCb simulation by dividing each Dalitz plot bin into many smaller cells, and using the BaBar amplitude model [5,6] to calculate the values of c_i and s_i within each cell. These values are then averaged together, weighted by the population of each cell after efficiency losses, to obtain an effective (c_i, s_i) for the bin as a whole, and the results compared with those determined assuming a flat efficiency. The differences between the two sets of results are found to be small compared with the CLEO-c measurement uncertainties. The data fit is then rerun many times, and the input values of (c_i, s_i) are smeared according to the size of these differences, and the mean shifts are assigned as a systematic uncertainty. These shifts vary between 0.2×10^{-2} and 0.3×10^{-2} .

The relative efficiency in each Dalitz plot bin is determined from the $B^{\pm} \rightarrow D\pi^{\pm}$ control sample. Biases can enter the measurement if there are differences in the relative acceptance over the Dalitz plot between the control sample and that of signal $B^{\pm} \rightarrow DK^{\pm}$ decays. Simulation studies show that the acceptance shapes are very similar between the two decays, but small variations exist which can be attributed to kinematic correlations in-

duced by the different PID requirements on the bachelor particle from the B decay. When included in the data fit, these variations induce biases that vary between 0.1×10^{-2} and 0.3×10^{-2} . In addition, a check is performed in which the control sample is fitted without combining together bins $+i$ and $-i$ in the efficiency calculation. As a result of this study small uncertainties of $\leq 0.3 \times 10^{-2}$ are assigned for the $D \rightarrow K_S^0 K^+ K^-$ measurement to account for possible biases induced by the difference in interaction cross-section for K^- and K^+ mesons interacting with the detector material. These contributions are combined together with the uncertainty arising from efficiency variation within a Dalitz plot bin to give the component labelled ‘Efficiency effects’ in Tables 4 and 5.

The use of the control channel to determine the relative efficiency on the Dalitz plot assumes that the amplitude of the suppressed tree diagram is negligible. If this is not the case then the B^- final state will receive a contribution from \bar{D}^0 decays, and this will lead to the presence of CP violation via the same mechanism as in $B \rightarrow DK$ decays. The size of any CP violation that exists in this channel is governed by $r_B^{D\pi}$, γ and $\delta_B^{D\pi}$, where the parameters with superscripts are analogous to their counterparts in $B^{\pm} \rightarrow DK^{\pm}$ decays. The naive expectation is that $r_B^{D\pi} \sim 0.005$ but larger values are possible, and the studies reported in Ref. [1] are compatible with this possibility. Therefore simulated experiments are performed with finite CP violation injected in the control channel, conservatively setting $r_B^{D\pi}$ to be 0.02, taking a wide variation in the value of the unknown strong-phase difference $\delta_B^{D\pi}$, and choosing $\gamma = 70^\circ$. The experiments are fit under the no CP violation hypothesis and the largest shifts observed are assigned as a systematic uncertainty. This contribution is the largest source of experimental systematic uncertainty in the measurement, for example contributing an error of 1.5×10^{-2} in the case of x_+ in the full data fit.

The resolution of each decay on the Dalitz plot is approximately $0.004 \text{ GeV}^2/c^4$ for candidates with long K_S^0 decays and $0.006 \text{ GeV}^2/c^4$ for those containing downstream K_S^0 in the m_+^2 and m_-^2 directions. This is small compared to the typical width of a bin, nonetheless some net migration is possible away from the more densely populated bins. At first order this effect is accounted for by use of the control channel, but residual effects enter because of the different distribution in the Dalitz plot of the signal events. Once more a series of simulated experiments is performed to assess the size of any possible bias which is found to vary between 0.2×10^{-2} and 0.4×10^{-2} .

The distribution of the partially reconstructed background is varied over the Dalitz plot according to the uncertainty in the make-up of this background component. From these studies an uncertainty of $(0.2-0.3) \times 10^{-2}$ is assigned to the fit parameters in the full data fit.

Two systematic uncertainties are evaluated that are associated with the misidentified $B^{\pm} \rightarrow D\pi^{\pm}$ background in the $B^{\pm} \rightarrow DK^{\pm}$ sample. Firstly, there is a 0.2×10^{-2} uncertainty on the knowledge of the efficiency of the PID cut that distinguishes pions from kaons. This is found to have only a small effect on the measured values of x_{\pm} and y_{\pm} . Secondly, it is possible that the invariant mass distribution of the misidentified background is not constant over the Dalitz plot, as is assumed in the fit. This can occur through kinematic correlations between the reconstruction efficiency on the Dalitz plot of the D decay and the momentum of the bachelor pion from the B^{\pm} decay. Simulated experiments are performed with different shapes input according to the Dalitz plot bin and the results of simulation studies, and these experiments are then fitted assuming a uniform shape, as in data. Uncertainties are assigned in the range $(0.1-0.3) \times 10^{-2}$.

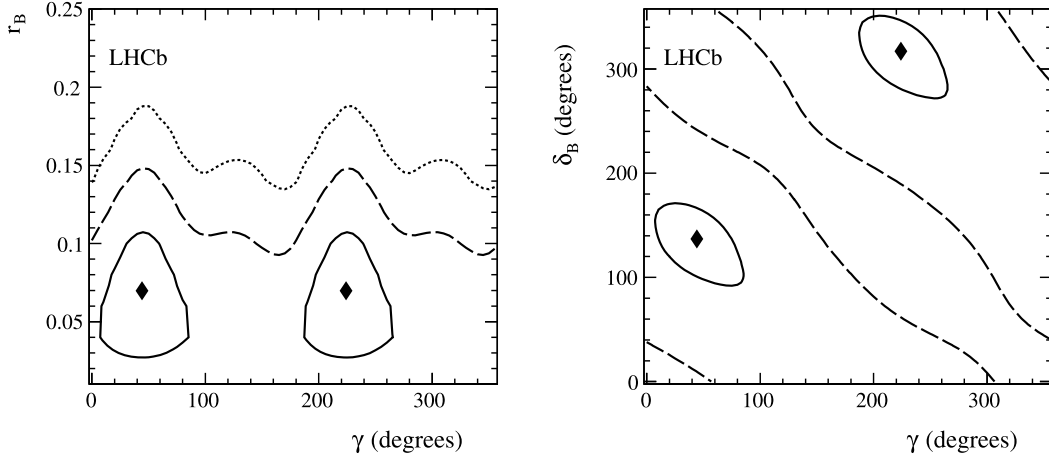


Fig. 7. Two-dimensional projections of confidence regions onto the (γ, r_B) and (γ, δ_B) planes showing the one (solid) and two (dashed) standard deviations with all uncertainties included. For the (γ, r_B) projection the three (dotted) standard deviation contour is also shown. The points mark the central values.

An uncertainty is assigned to each parameter to accompany the correction that is applied for the small bias which is present in the fit procedure. These uncertainties are determined by performing sets of simulated experiments, in each of which different values of x_{\pm} and y_{\pm} are input, corresponding to a range that is wide compared to the current experimental knowledge, and also encompassing the results of this analysis. The spread in observed bias is taken as the systematic error, and is largest for y_+ , reaching a value of 0.5×10^{-2} in the full data fit.

Finally, several robustness checks are conducted to assess the stability of the results. These include repeating the analysis with alternative binning schemes for the $D \rightarrow K_S^0 \pi^+ \pi^-$ data and performing the fits without making any distinction between K_S^0 category. These tests return results compatible with the baseline procedure.

The total experimental systematic uncertainty from LHCb-related sources is determined to be 1.5×10^{-2} on x_- , 0.9×10^{-2} on y_- , 1.8×10^{-2} on x_+ and 0.8×10^{-2} on y_+ . These are all smaller than the corresponding statistical uncertainties. The dominant contribution arises from allowing for the possibility of CP violation in the control channel, $B \rightarrow D\pi$. In the future, when larger data sets are analysed, alternative analysis methods will be explored to eliminate this potential source of bias.

The limited precision on (c_i, s_i) coming from the CLEO-c measurement induces uncertainties on x_{\pm} and y_{\pm} [12]. These uncertainties are evaluated by rerunning the data fit many times, and smearing the input values of (c_i, s_i) according to their measurement errors and correlations. Values of $(0.6\text{--}3.0) \times 10^{-2}$ are found for the fit to the full sample. When evaluated for the $D \rightarrow K_S^0 \pi^+ \pi^-$ data set alone, the results are similar in magnitude, but not identical, to those reported in the corresponding Belle analysis [13]. Differences are to be expected, as these uncertainties have a dependence on the central values of the x_{\pm} and y_{\pm} parameters, and are sample-dependent for small data sets. Simulation studies indicate that these uncertainties will be reduced when larger $B^{\pm} \rightarrow DK^{\pm}$ data sets are analysed.

After taking account of all sources of uncertainty the correlation coefficient between x_- and y_- in the full fit is calculated to be -0.10 and that between x_+ and y_+ to be 0.22 . The correlations between B^- and B^+ parameters are found to be small and can be neglected. These correlations are summarised in Table 3, together with those coming from the statistical uncertainties alone, and those from the fit to $D \rightarrow K_S^0 \pi^+ \pi^-$ data.

7. Interpretation

The results for x_{\pm} and y_{\pm} can be interpreted in terms of the underlying physics parameters γ , r_B and δ_B . This is done using a frequentist approach with Feldman–Cousins ordering [27], using the same procedure as described in Ref. [13]. In this manner confidence levels are obtained for the three physics parameters. The confidence levels for one, two and three standard deviations are taken at 20%, 74% and 97%, which is appropriate for a three-dimensional Gaussian distribution. The projections of the three-dimensional surfaces bounding the one, two and three standard deviation volumes onto the (γ, r_B) and (γ, δ_B) planes are shown in Fig. 7. The LHCb-related systematic uncertainties are taken as uncorrelated and correlations of the CLEO-c and statistical uncertainties are taken into account. The statistical and systematic uncertainties on x and y are combined in quadrature.

The solution for the physics parameters has a two-fold ambiguity, (γ, δ_B) and $(\gamma + 180^\circ, \delta_B + 180^\circ)$. Choosing the solution that satisfies $0 < \gamma < 180^\circ$ yields $r_B = 0.07 \pm 0.04$, $\gamma = (44_{-38}^{+43})^\circ$ and $\delta_B = (137_{-46}^{+35})^\circ$. The value for r_B is consistent with, but lower than, the world average of results from previous experiments [15]. This low value means that it is not possible to use the results of this analysis, in isolation, to set strong constraints on the values of γ and δ_B , as can be seen by the large uncertainties on these parameters.

8. Conclusions

Approximately 800 $B^{\pm} \rightarrow DK^{\pm}$ decay candidates, with the D meson decaying either to $K_S^0 \pi^+ \pi^-$ or $K_S^0 K^+ K^-$, have been selected from 1.0 fb^{-1} of data collected by LHCb in 2011. These samples have been analysed to determine the CP-violating parameters $x_{\pm} = r_B \cos(\delta_B \pm \gamma)$ and $y_{\pm} = r_B \sin(\delta_B \pm \gamma)$, where r_B is the ratio of the absolute values of the $B^+ \rightarrow D^0 K^-$ and $B^+ \rightarrow \bar{D}^0 K^-$ amplitudes, δ_B is the strong-phase difference between them, and γ is the angle of the unitarity triangle. The analysis is performed in bins of D decay Dalitz space and existing measurements of the CLEO-c experiment are used to provide input on the D decay strong-phase parameters (c_i, s_i) [12]. Such an approach allows the analysis to be essentially independent of any model-dependent assumptions on the strong-phase variation across Dalitz space. It is the first time this method has been applied to $D \rightarrow K_S^0 K^+ K^-$ decays. The following results are obtained

$$x_- = (0.0 \pm 4.3 \pm 1.5 \pm 0.6) \times 10^{-2},$$

$$y_- = (2.7 \pm 5.2 \pm 0.8 \pm 2.3) \times 10^{-2},$$

$$x_+ = (-10.3 \pm 4.5 \pm 1.8 \pm 1.4) \times 10^{-2},$$

$$y_+ = (-0.9 \pm 3.7 \pm 0.8 \pm 3.0) \times 10^{-2},$$

where the first uncertainty is statistical, the second is systematic and the third arises from the experimental knowledge of the (c_i, s_i) parameters. These values have similar precision to those obtained in a recent binned study by the Belle experiment [13].

When interpreting these results in terms of the underlying physics parameters it is found that $r_B = 0.07 \pm 0.04$, $\gamma = (44^{+43}_{-38})^\circ$ and $\delta_B = (137^{+35}_{-46})^\circ$. These values are consistent with the world average of results from previous measurements [15], although the uncertainties on γ and δ_B are large. This is partly driven by the relatively low central value that is obtained for the parameter r_B . More stringent constraints are expected when these results are combined with other measurements from LHCb which have complementary sensitivity to the same physics parameters.

Acknowledgements

We express our gratitude to our colleagues in the CERN accelerator departments for the excellent performance of the LHC. We thank the technical and administrative staff at CERN and at the LHCb institutes, and acknowledge support from the National Agencies: CAPES, CNPq, FAPERJ and FINEP (Brazil); CERN; NSFC (China); CNRS/IN2P3 (France); BMBF, DFG, HGF and MPG (Germany); SFI (Ireland); INFN (Italy); FOM and NWO (The Netherlands); SCSR (Poland); ANCS (Romania); MinES of Russia and Rosatom (Russia); MICINN, XuntaGal and GENCAT (Spain); SNSF and SER (Switzerland); NAS Ukraine (Ukraine); STFC (United Kingdom); NSF (USA). We also acknowledge the support received from the ERC under FP7 and the Region Auvergne.

Open access

This article is published Open Access at [sciencedirect.com](http://www.sciencedirect.com). It is distributed under the terms of the Creative Commons Attribution License 3.0, which permits unrestricted use, distribution, and reproduction in any medium, provided the original authors and source are credited.

LHCb Collaboration

R. Aaij³⁸, C. Abellan Beteta^{33,n}, A. Adametz¹¹, B. Adeva³⁴, M. Adinolfi⁴³, C. Adrover⁶, A. Affolder⁴⁹, Z. Ajaltouni⁵, J. Albrecht³⁵, F. Alessio³⁵, M. Alexander⁴⁸, S. Ali³⁸, G. Alkhazov²⁷, P. Alvarez Cartelle³⁴, A.A. Alves Jr.²², S. Amato², Y. Amhis³⁶, L. Anderlini^{17,f}, J. Anderson³⁷, R.B. Appleby⁵¹, O. Aquines Gutierrez¹⁰, F. Archilli^{18,35}, A. Artamonov³², M. Artuso⁵³, E. Aslanides⁶, G. Auriemma^{22,m}, S. Bachmann¹¹, J.J. Back⁴⁵, C. Baesso⁵⁴, W. Baldini¹⁶, R.J. Barlow⁵¹, C. Barschel³⁵, S. Barsuk⁷, W. Barter⁴⁴, A. Bates⁴⁸, Th. Bauer³⁸, A. Bay³⁶, J. Beddow⁴⁸, I. Bediaga¹, S. Belogurov²⁸, K. Belous³², I. Belyaev²⁸, E. Ben-Haim⁸, M. Benayoun⁸, G. Bencivenni¹⁸, S. Benson⁴⁷, J. Benton⁴³, A. Berezhnoy²⁹, R. Bernet³⁷, M.-O. Bettler⁴⁴, M. van Beuzekom³⁸, A. Bien¹¹, S. Bifani¹², T. Bird⁵¹, A. Bizzeti^{17,h}, P.M. Björnstad⁵¹, T. Blake³⁵, F. Blanc³⁶, C. Blanks⁵⁰, J. Blouw¹¹, S. Blusk⁵³, A. Bobrov³¹, V. Bocci²², A. Bondar³¹, N. Bondar²⁷, W. Bonivento¹⁵, S. Borghi^{48,51}, A. Borgia⁵³, T.J.V. Bowcock⁴⁹, C. Bozzi¹⁶, T. Brambach⁹, J. van den Brand³⁹, J. Bressieux³⁶, D. Brett⁵¹, M. Britsch¹⁰, T. Britton⁵³, N.H. Brook⁴³, H. Brown⁴⁹, A. Büchler-Germann³⁷, I. Burducea²⁶, A. Bursche³⁷, J. Buytaert³⁵, S. Cadeddu¹⁵, O. Callot⁷, M. Calvi^{20,j}, M. Calvo Gomez^{33,n}, A. Camboni³³, P. Campana^{18,35}, A. Carbone^{14,c}, G. Carboni^{21,k}, R. Cardinale^{19,i}, A. Cardini¹⁵, L. Carson⁵⁰, K. Carvalho Akiba², G. Casse⁴⁹, M. Cattaneo³⁵, Ch. Cauet⁹, M. Charles⁵², Ph. Charpentier³⁵, P. Chen^{3,36}, N. Chiapolini³⁷, M. Chrzaszcz²³, K. Ciba³⁵, X. Cid Vidal³⁴,

References

- [1] LHCb Collaboration, R. Aaij, et al., Phys. Lett. B 712 (2012) 203, arXiv:1203.3662.
- [2] A. Giri, Y. Grossman, A. Softer, J. Zupan, Phys. Rev. D 68 (2003) 054018, arXiv:hep-ph/0303187.
- [3] A. Bondar, Proceedings of BINP special analysis meeting on Dalitz analysis, 24–26 Sep. 2002, unpublished.
- [4] BaBar Collaboration, B. Aubert, et al., Phys. Rev. Lett. 95 (2005) 121802, arXiv:hep-ex/0504039.
- [5] BaBar Collaboration, B. Aubert, et al., Phys. Rev. D 78 (2008) 034023, arXiv:0804.2089.
- [6] BaBar Collaboration, P. del Amo Sanchez, et al., Phys. Rev. Lett. 105 (2010) 121801, arXiv:1005.1096.
- [7] Belle Collaboration, A. Poluektov, et al., Phys. Rev. D 70 (2004) 072003, arXiv:hep-ex/0406067.
- [8] Belle Collaboration, A. Poluektov, et al., Phys. Rev. D 73 (2006) 112009, arXiv:hep-ex/0604054.
- [9] Belle Collaboration, A. Poluektov, et al., Phys. Rev. D 81 (2010) 112002, arXiv:1003.3360.
- [10] A. Bondar, A. Poluektov, Eur. Phys. J. C 47 (2006) 347, arXiv:hep-ph/0510246.
- [11] A. Bondar, A. Poluektov, Eur. Phys. J. C 55 (2008) 51, arXiv:0801.0840.
- [12] CLEO Collaboration, J. Libby, et al., Phys. Rev. D 82 (2010) 112006, arXiv:1010.2817.
- [13] Belle Collaboration, H. Aihara, et al., Phys. Rev. D 85 (2012) 112014, arXiv:1204.6561.
- [14] Heavy Flavor Averaging Group, D. Asner, et al., Averages of b-hadron, c-hadron, and τ -lepton properties, arXiv:1010.1589, updates available online at <http://www.slac.stanford.edu/xorg/hfag>.
- [15] Particle Data Group, J. Beringer, et al., Phys. Rev. D 86 (2012) 010001.
- [16] A. Bondar, A. Poluektov, V. Vorobiev, Phys. Rev. D 82 (2010) 034033, arXiv:1004.2350.
- [17] LHCb Collaboration, A.A. Alves Jr., et al., JINST 3 (2008) S08005.
- [18] V.V. Gligorov, C. Thomas, M. Williams, The HIT inclusive B triggers, LHCb-PUB-2011-016.
- [19] T. Sjöstrand, S. Mrenna, P. Skands, JHEP 0605 (2006) 026, arXiv:hep-ph/0603175.
- [20] I. Belyaev, et al., in: Nuclear Science Symposium Conference Record (NSS/MIC), IEEE, 2010, p. 1155.
- [21] D.J. Lange, Nucl. Instrum. Meth. A 462 (2001) 152.
- [22] P. Golonka, Z. Was, Eur. Phys. J. C 45 (2006) 97, arXiv:hep-ph/0506026.
- [23] GEANT4 Collaboration, J. Allison, et al., IEEE Trans. Nucl. Sci. 53 (2006) 270; GEANT4 Collaboration, S. Agostinelli, et al., Nucl. Instrum. Meth. A 506 (2003) 250.
- [24] M. Clemencic, et al., J. Phys.: Conf. Ser. 331 (2011) 032023.
- [25] K.S. Cranmer, Comput. Phys. Comm. 136 (2001) 198, arXiv:hep-ex/0011057.
- [26] T. Skwarnicki, A study of the radiative cascade transitions between the Upsilon-prime and Upsilon resonances, PhD thesis, Institute of Nuclear Physics, Krakow, 1986, DESY-F31-86-02.
- [27] G.J. Feldman, R.D. Cousins, Phys. Rev. D 57 (1998) 3873, arXiv:physics/9711021.

G. Ciezarek⁵⁰, P.E.L. Clarke⁴⁷, M. Clemencic³⁵, H.V. Cliff⁴⁴, J. Closier³⁵, C. Coca²⁶, V. Coco³⁸, J. Cogan⁶, E. Cogneras⁵, P. Collins³⁵, A. Comerma-Montells³³, A. Contu^{52,15}, A. Cook⁴³, M. Coombes⁴³, G. Corti³⁵, B. Couturier³⁵, G.A. Cowan³⁶, D. Craik⁴⁵, S. Cunliffe⁵⁰, R. Currie⁴⁷, C. D'Ambrosio³⁵, P. David⁸, P.N.Y. David³⁸, I. De Bonis⁴, K. De Bruyn³⁸, S. De Capua^{21,k}, M. De Cian³⁷, J.M. De Miranda¹, L. De Paula², P. De Simone¹⁸, D. Decamp⁴, M. Deckenhoff⁹, H. Degaudenzi^{36,35}, L. Del Buono⁸, C. Deplano¹⁵, D. Derkach¹⁴, O. Deschamps⁵, F. Dettori³⁹, A. Di Canto¹¹, J. Dickens⁴⁴, H. Dijkstra³⁵, P. Diniz Batista¹, F. Domingo Bonal^{33,n}, S. Donleavy⁴⁹, F. Dordei¹¹, A. Dosil Suárez³⁴, D. Dossett⁴⁵, A. Dovbnya⁴⁰, F. Dupertuis³⁶, R. Dzhelyadin³², A. Dziurda²³, A. Dzyuba²⁷, S. Easo⁴⁶, U. Egede⁵⁰, V. Egorychev²⁸, S. Eidelman³¹, D. van Eijk³⁸, S. Eisenhardt⁴⁷, R. Ekelhof⁹, L. Eklund⁴⁸, I. El Rifai⁵, Ch. Elsasser³⁷, D. Elsby⁴², D. Esperante Pereira³⁴, A. Falabella^{14,e}, C. Färber¹¹, G. Fardell⁴⁷, C. Farinelli³⁸, S. Farry¹², V. Fave³⁶, V. Fernandez Albor³⁴, F. Ferreira Rodrigues¹, M. Ferro-Luzzi³⁵, S. Filippov³⁰, C. Fitzpatrick³⁵, M. Fontana¹⁰, F. Fontanelli^{19,i}, R. Forty³⁵, O. Francisco², M. Frank³⁵, C. Frei³⁵, M. Frosini^{17,f}, S. Furcas²⁰, A. Gallas Torreira³⁴, D. Galli^{14,c}, M. Gandelman², P. Gandini⁵², Y. Gao³, J.-C. Garnier³⁵, J. Garofoli⁵³, P. Garosi⁵¹, J. Garra Tico⁴⁴, L. Garrido³³, C. Gaspar³⁵, R. Gauld⁵², E. Gersabeck¹¹, M. Gersabeck³⁵, T. Gershon^{45,35}, Ph. Ghez⁴, V. Gibson⁴⁴, V.V. Gligorov³⁵, C. Göbel⁵⁴, D. Golubkov²⁸, A. Golutvin^{50,28,35}, A. Gomes², H. Gordon⁵², M. Grabalosa Gándara³³, R. Graciani Diaz³³, L.A. Granado Cardoso³⁵, E. Graugés³³, G. Graziani¹⁷, A. Greco²⁶, E. Greening⁵², S. Gregson⁴⁴, O. Grünberg⁵⁵, B. Gui⁵³, E. Gushchin³⁰, Yu. Guz³², T. Gys³⁵, C. Hadjivasiliou⁵³, G. Haefeli³⁶, C. Haen³⁵, S.C. Haines⁴⁴, S. Hall⁵⁰, T. Hampson⁴³, S. Hansmann-Menzemer¹¹, N. Harnew⁵², S.T. Harnew⁴³, J. Harrison⁵¹, P.F. Harrison⁴⁵, T. Hartmann⁵⁵, J. He⁷, V. Heijne³⁸, K. Hennessy⁴⁹, P. Henrard⁵, J.A. Hernando Morata³⁴, E. van Herwijnen³⁵, E. Hicks⁴⁹, D. Hill⁵², M. Hoballah⁵, P. Hopchev⁴, W. Hulsbergen³⁸, P. Hunt⁵², T. Huse⁴⁹, N. Hussain⁵², D. Hutchcroft⁴⁹, D. Hynds⁴⁸, V. Iakovenko⁴¹, P. Ilten¹², J. Imong⁴³, R. Jacobsson³⁵, A. Jaeger¹¹, M. Jahjah Hussein⁵, E. Jans³⁸, F. Jansen³⁸, P. Jaton³⁶, B. Jean-Marie⁷, F. Jing³, M. John⁵², D. Johnson⁵², C.R. Jones⁴⁴, B. Jost³⁵, M. Kabbalo⁹, S. Kandybei⁴⁰, M. Karacson³⁵, T.M. Karbach⁹, J. Keaveney¹², I.R. Kenyon⁴², U. Kerzel³⁵, T. Ketel³⁹, A. Keune³⁶, B. Khanji²⁰, Y.M. Kim⁴⁷, O. Kochebina⁷, V. Komarov^{36,29}, R.F. Koopman³⁹, P. Koppenburg³⁸, M. Korolev²⁹, A. Kozlinskiy³⁸, L. Kravchuk³⁰, K. Kreplin¹¹, M. Kreps⁴⁵, G. Krocker¹¹, P. Krokovny³¹, F. Kruse⁹, M. Kucharczyk^{20,23,j}, V. Kudryavtsev³¹, T. Kvaratskheliya^{28,35}, V.N. La Thi³⁶, D. Lacarrere³⁵, G. Lafferty⁵¹, A. Lai¹⁵, D. Lambert⁴⁷, R.W. Lambert³⁹, E. Lanciotti³⁵, G. Lanfranchi^{18,35}, C. Langenbruch³⁵, T. Latham⁴⁵, C. Lazzeroni⁴², R. Le Gac⁶, J. van Leerdam³⁸, J.-P. Lees⁴, R. Lefèvre⁵, A. Leflat^{29,35}, J. Lefrançois⁷, O. Leroy⁶, T. Lesiak²³, Y. Li³, L. Li Gioi⁵, M. Liles⁴⁹, R. Lindner³⁵, C. Linn¹¹, B. Liu³, G. Liu³⁵, J. von Loeben²⁰, J.H. Lopes², E. Lopez Asamar³³, N. Lopez-March³⁶, H. Lu³, J. Luisier³⁶, A. Mac Raighne⁴⁸, F. Machefert⁷, I.V. Machikhiliyan^{4,28}, F. Maciuc²⁶, O. Maev^{27,35}, J. Magnin¹, M. Maino²⁰, S. Malde⁵², G. Manca^{15,d}, G. Mancinelli⁶, N. Mangiafave⁴⁴, U. Marconi¹⁴, R. Märki³⁶, J. Marks¹¹, G. Martellotti²², A. Martens⁸, L. Martin⁵², A. Martín Sánchez⁷, M. Martinelli³⁸, D. Martinez Santos³⁵, A. Massafferri¹, Z. Mathe³⁵, C. Matteuzzi²⁰, M. Matveev²⁷, E. Maurice⁶, A. Mazurov^{16,30,35}, J. McCarthy⁴², G. McGregor⁵¹, R. McNulty¹², M. Meissner¹¹, M. Merk³⁸, J. Merkel⁹, D.A. Milanes¹³, M.-N. Minard⁴, J. Molina Rodriguez⁵⁴, S. Monteil⁵, D. Moran⁵¹, P. Morawski²³, R. Mountain⁵³, I. Mous³⁸, F. Muheim⁴⁷, K. Müller³⁷, R. Muresan²⁶, B. Muryn²⁴, B. Muster³⁶, J. Mylroie-Smith⁴⁹, P. Naik⁴³, T. Nakada³⁶, R. Nandakumar⁴⁶, I. Nasteva¹, M. Needham⁴⁷, N. Neufeld³⁵, A.D. Nguyen³⁶, C. Nguyen-Mau^{36,o}, M. Nicol⁷, V. Niess⁵, N. Nikitin²⁹, T. Nikodem¹¹, A. Nomerotski^{52,35}, A. Novoselov³², A. Oblakowska-Mucha²⁴, V. Obraztsov³², S. Oggero³⁸, S. Ogilvy⁴⁸, O. Okhrimenko⁴¹, R. Oldeman^{15,35,d}, M. Orlandea²⁶, J.M. Otalora Goicochea², P. Owen⁵⁰, B.K. Pal⁵³, A. Palano^{13,b}, M. Palutan¹⁸, J. Panman³⁵, A. Papanestis⁴⁶, M. Pappagallo⁴⁸, C. Parkes⁵¹, C.J. Parkinson⁵⁰, G. Passaleva¹⁷, G.D. Patel⁴⁹, M. Patel⁵⁰, G.N. Patrick⁴⁶, C. Patrignani^{19,i}, C. Pavel-Nicorescu²⁶, A. Pazos Alvarez³⁴, A. Pellegrino³⁸, G. Penso^{22,l}, M. Pepe Altarelli³⁵, S. Perazzini^{14,c}, D.L. Perego^{20,j}, E. Perez Trigo³⁴, A. Pérez-Calero Yzquierdo³³, P. Perret⁵, M. Perrin-Terrin⁶, G. Pessina²⁰, K. Petridis⁵⁰, A. Petrolini^{19,i}, A. Phan⁵³, E. Picatoste Olloqui³³, B. Pie Valls³³, B. Pietrzyk⁴, T. Pilař⁴⁵, D. Pinci²², S. Playfer⁴⁷, M. Plo Casasus³⁴, F. Polci⁸, G. Polok²³, A. Poluektov^{45,31}, E. Polcarpo², D. Popov¹⁰, B. Popovici²⁶, C. Potterat³³, A. Powell⁵², J. Prisciandaro³⁶, V. Pugatch⁴¹, A. Puig Navarro³⁶, W. Qian³, J.H. Rademacker⁴³, B. Rakotomiamanana³⁶, M.S. Rangel², I. Raniuk⁴⁰, N. Rauschmayr³⁵, G. Raven³⁹, S. Redford⁵²,

M.M. Reid⁴⁵, A.C. dos Reis¹, S. Ricciardi⁴⁶, A. Richards⁵⁰, K. Rinnert⁴⁹, V. Rives Molina³³, D.A. Roa Romero⁵, P. Robbe⁷, E. Rodrigues^{48,51}, P. Rodriguez Perez³⁴, G.J. Rogers⁴⁴, S. Roiser³⁵, V. Romanovsky³², A. Romero Vidal³⁴, J. Rouvinet³⁶, T. Ruf³⁵, H. Ruiz³³, G. Sabatino^{21,k}, J.J. Saborido Silva³⁴, N. Sagidova²⁷, P. Sail⁴⁸, B. Saitta^{15,d}, C. Salzmann³⁷, B. Sanmartin Sedes³⁴, M. Sannino^{19,i}, R. Santacesaria²², C. Santamarina Rios³⁴, R. Santinelli³⁵, E. Santovetti^{21,k}, M. Sapunov⁶, A. Sarti^{18,l}, C. Satriano^{22,m}, A. Satta²¹, M. Savrie^{16,e}, P. Schaack⁵⁰, M. Schiller³⁹, H. Schindler³⁵, S. Schleich⁹, M. Schlupp⁹, M. Schmelling¹⁰, B. Schmidt³⁵, O. Schneider³⁶, A. Schopper³⁵, M.-H. Schune⁷, R. Schwemmer³⁵, B. Sciascia¹⁸, A. Sciubba^{18,l}, M. Seco³⁴, A. Semennikov²⁸, K. Senderowska²⁴, I. Sepp⁵⁰, N. Serra³⁷, J. Serrano⁶, P. Seyfert¹¹, M. Shapkin³², I. Shapoval^{40,35}, P. Shatalov²⁸, Y. Shcheglov²⁷, T. Shears^{49,35}, L. Shekhtman³¹, O. Shevchenko⁴⁰, V. Shevchenko²⁸, A. Shires⁵⁰, R. Silva Coutinho⁴⁵, T. Skwarnicki⁵³, N.A. Smith⁴⁹, E. Smith^{52,46}, M. Smith⁵¹, K. Sobczak⁵, F.J.P. Soler⁴⁸, F. Soomro^{18,35}, D. Souza⁴³, B. Souza De Paula², B. Spaan⁹, A. Sparkes⁴⁷, P. Spradlin⁴⁸, F. Stagni³⁵, S. Stahl¹¹, O. Steinkamp³⁷, S. Stoica²⁶, S. Stone⁵³, B. Storaci³⁸, M. Straticiu²⁶, U. Straumann³⁷, V.K. Subbiah³⁵, S. Swientek⁹, M. Szczekowski²⁵, P. Szczypka^{36,35}, T. Szumlak²⁴, S. T'Jampens⁴, M. Teklishyn⁷, E. Teodorescu²⁶, F. Teubert³⁵, C. Thomas⁵², E. Thomas³⁵, J. van Tilburg¹¹, V. Tisserand⁴, M. Tobin³⁷, S. Tolk³⁹, D. Tonelli³⁵, S. Topp-Joergensen⁵², N. Torr⁵², E. Tournefier^{4,50}, S. Tourneur³⁶, M.T. Tran³⁶, A. Tsaregorodtsev⁶, P. Tsoelas³⁸, N. Tuning³⁸, M. Ubeda Garcia³⁵, A. Ukleja²⁵, D. Urner⁵¹, U. Uwer¹¹, V. Vagnoni¹⁴, G. Valenti¹⁴, R. Vazquez Gomez³³, P. Vazquez Regueiro³⁴, S. Vecchi¹⁶, J.J. Velthuis⁴³, M. Veltri^{17,g}, G. Veneziano³⁶, M. Vesterinen³⁵, B. Viaud⁷, I. Videau⁷, D. Vieira², X. Vilasis-Cardona^{33,n}, J. Visniakov³⁴, A. Vollhardt³⁷, D. Volyanskyy¹⁰, D. Voong⁴³, A. Vorobyev²⁷, V. Vorobyev³¹, H. Voss¹⁰, C. Voß⁵⁵, R. Waldi⁵⁵, R. Wallace¹², S. Wandernoth¹¹, J. Wang⁵³, D.R. Ward⁴⁴, N.K. Watson⁴², A.D. Webber⁵¹, D. Websdale⁵⁰, M. Whitehead⁴⁵, J. Wicht³⁵, D. Wiedner¹¹, L. Wiggers³⁸, G. Wilkinson^{52,*}, M.P. Williams^{45,46}, M. Williams^{50,p}, F.F. Wilson⁴⁶, J. Wishahi⁹, M. Witek^{23,35}, W. Witzeling³⁵, S.A. Wotton⁴⁴, S. Wright⁴⁴, S. Wu³, K. Wyllie³⁵, Y. Xie⁴⁷, F. Xing⁵², Z. Xing⁵³, Z. Yang³, R. Young⁴⁷, X. Yuan³, O. Yushchenko³², M. Zangoli¹⁴, M. Zavertyaev^{10,a}, F. Zhang³, L. Zhang⁵³, W.C. Zhang¹², Y. Zhang³, A. Zhelezov¹¹, L. Zhong³, A. Zvyagin³⁵

¹ Centro Brasileiro de Pesquisas Físicas (CBPF), Rio de Janeiro, Brazil

² Universidade Federal do Rio de Janeiro (UFRJ), Rio de Janeiro, Brazil

³ Center for High Energy Physics, Tsinghua University, Beijing, China

⁴ LAPP, Université de Savoie, CNRS/IN2P3, Annecy-Le-Vieux, France

⁵ Clermont Université, Université Blaise Pascal, CNRS/IN2P3, LPC, Clermont-Ferrand, France

⁶ CPPM, Aix-Marseille Université, CNRS/IN2P3, Marseille, France

⁷ LAL, Université Paris-Sud, CNRS/IN2P3, Orsay, France

⁸ LPNHE, Université Pierre et Marie Curie, Université Paris Diderot, CNRS/IN2P3, Paris, France

⁹ Fakultät Physik, Technische Universität Dortmund, Dortmund, Germany

¹⁰ Max-Planck-Institut für Kernphysik (MPIK), Heidelberg, Germany

¹¹ Physikalisches Institut, Ruprecht-Karls-Universität Heidelberg, Heidelberg, Germany

¹² School of Physics, University College Dublin, Dublin, Ireland

¹³ Sezione INFN di Bari, Bari, Italy

¹⁴ Sezione INFN di Bologna, Bologna, Italy

¹⁵ Sezione INFN di Cagliari, Cagliari, Italy

¹⁶ Sezione INFN di Ferrara, Ferrara, Italy

¹⁷ Sezione INFN di Firenze, Firenze, Italy

¹⁸ Laboratori Nazionali dell'INFN di Frascati, Frascati, Italy

¹⁹ Sezione INFN di Genova, Genova, Italy

²⁰ Sezione INFN di Milano Bicocca, Milano, Italy

²¹ Sezione INFN di Roma Tor Vergata, Roma, Italy

²² Sezione INFN di Roma La Sapienza, Roma, Italy

²³ Henryk Niewodniczanski Institute of Nuclear Physics, Polish Academy of Sciences, Kraków, Poland

²⁴ AGH University of Science and Technology, Kraków, Poland

²⁵ National Center for Nuclear Research (NCBJ), Warsaw, Poland

²⁶ Horia Hulubei National Institute of Physics and Nuclear Engineering, Bucharest-Magurele, Romania

²⁷ Petersburg Nuclear Physics Institute (PNPI), Gatchina, Russia

²⁸ Institute of Theoretical and Experimental Physics (ITEP), Moscow, Russia

²⁹ Institute of Nuclear Physics, Moscow State University (SINP MSU), Moscow, Russia

³⁰ Institute for Nuclear Research of the Russian Academy of Sciences (INR RAN), Moscow, Russia

³¹ Budker Institute of Nuclear Physics (SB RAS) and Novosibirsk State University, Novosibirsk, Russia

³² Institute for High Energy Physics (IHEP), Protvino, Russia

³³ Universitat de Barcelona, Barcelona, Spain

³⁴ Universidad de Santiago de Compostela, Santiago de Compostela, Spain

³⁵ European Organization for Nuclear Research (CERN), Geneva, Switzerland

³⁶ Ecole Polytechnique Fédérale de Lausanne (EPFL), Lausanne, Switzerland

³⁷ Physik-Institut, Universität Zürich, Zürich, Switzerland

- ³⁸ Nikhef National Institute for Subatomic Physics, Amsterdam, The Netherlands
³⁹ Nikhef National Institute for Subatomic Physics and VU University Amsterdam, Amsterdam, The Netherlands
⁴⁰ NSC Kharkiv Institute of Physics and Technology (NSC KIPT), Kharkiv, Ukraine
⁴¹ Institute for Nuclear Research of the National Academy of Sciences (KINR), Kyiv, Ukraine
⁴² University of Birmingham, Birmingham, United Kingdom
⁴³ H.H. Wills Physics Laboratory, University of Bristol, Bristol, United Kingdom
⁴⁴ Cavendish Laboratory, University of Cambridge, Cambridge, United Kingdom
⁴⁵ Department of Physics, University of Warwick, Coventry, United Kingdom
⁴⁶ STFC Rutherford Appleton Laboratory, Didcot, United Kingdom
⁴⁷ School of Physics and Astronomy, University of Edinburgh, Edinburgh, United Kingdom
⁴⁸ School of Physics and Astronomy, University of Glasgow, Glasgow, United Kingdom
⁴⁹ Oliver Lodge Laboratory, University of Liverpool, Liverpool, United Kingdom
⁵⁰ Imperial College London, London, United Kingdom
⁵¹ School of Physics and Astronomy, University of Manchester, Manchester, United Kingdom
⁵² Department of Physics, University of Oxford, Oxford, United Kingdom
⁵³ Syracuse University, Syracuse, NY, United States
⁵⁴ Pontifícia Universidade Católica do Rio de Janeiro (PUC-Rio), Rio de Janeiro, Brazil ^q
⁵⁵ Institut für Physik, Universität Rostock, Rostock, Germany ^r

* Corresponding author.

E-mail address: guy.wilkinson@cern.ch (G. Wilkinson).

- ^a P.N. Lebedev Physical Institute, Russian Academy of Science (LPI RAS), Moscow, Russia.
^b Università di Bari, Bari, Italy.
^c Università di Bologna, Bologna, Italy.
^d Università di Cagliari, Cagliari, Italy.
^e Università di Ferrara, Ferrara, Italy.
^f Università di Firenze, Firenze, Italy.
^g Università di Urbino, Urbino, Italy.
^h Università di Modena e Reggio Emilia, Modena, Italy.
ⁱ Università di Genova, Genova, Italy.
^j Università di Milano Bicocca, Milano, Italy.
^k Università di Roma Tor Vergata, Roma, Italy.
^l Università di Roma La Sapienza, Roma, Italy.
^m Università della Basilicata, Potenza, Italy.
ⁿ LIFAELS, La Salle, Universitat Ramon Llull, Barcelona, Spain.
^o Hanoi University of Science, Hanoi, Viet Nam.
^p Massachusetts Institute of Technology, Cambridge, MA, United States.
^q Associated to Universidade Federal do Rio de Janeiro (UFRJ), Rio de Janeiro, Brazil.
^r Associated to Physikalisches Institut, Ruprecht-Karls-Universität Heidelberg, Heidelberg, Germany.